Highly dispersed platinum nanoparticles on carbon nanocoils and their electrocatalytic performance for fuel cell reactions

M. Sevilla,[a] *C. Sanchís,*[b] *T. Valdés-Solís,*[a] *E. Morallón*[b] *and A. B. Fuertes*[*a]

[a] Instituto Nacional del Carbón (CSIC), P. O. Box 73, 33080-Oviedo, Spain

[b] Departamento de Química Física e Instituto Universitario de Materiales. Universidad de Alicante. Apartado 99. 03080-Alicante. Spain

[*] **Corresponding author.** Tel.: +34 985119090. Fax : +34 985297662. E-mail**:** abefu@incar.csic.es

Abstract

Highly graphitic carbon nanocoils (GCNC) were synthesized through the catalytic graphitization of carbon microspheres obtained by the hydrothermal carbonization of different saccharides (sucrose, glucose and starch) and were used as a support for Pt nanoparticles. The Pt nanoparticles were deposited by means of a polymer mediated-polyol method. The Pt catalysts were characterized both physically (XRD, TEM, HRTEM and XPS) and electrochemically (electrooxidation of methanol in an acid medium). The electrocatalysts thus prepared show a high dispersion of Pt nanoparticles, with diameters in the 3.0-3.3 nm range and a very narrow particle size distribution. These catalytic systems possess high electroactive Pt surface areas (up to 85 $m^2 \cdot g^{-1}$ Pt) and they exhibit large catalytic activities towards methanol electrooxidation (up to 201 $A \cdot g^{-1}$ Pt). Moreover, they have a high resistance against oxidation, which is considerably greater than that of the Pt/Vulcan system.

Keywords: carbon nanostructures, Pt nanoparticles, electrocatalyst, methanol electrooxidation, voltammetry.

1. Introduction

Polymer electrolyte and direct methanol fuel cells (PEMFC and DMFC) are very promising candidates for vehicle and other portable applications due to their quick start-up, compactness and light weight, high power density and simplicity. However, the main barriers for the commercial utilization of these devices are the high cost and short durability of the catalyst (Pt), which is used to initiate the reactions both in the anode and cathode. Intensive research is being conducted to develop a suitable carbon support, which can provide high dispersions of Pt nanoparticles and a good stability against corrosion (oxidation). The combination of both of these properties is important because such a catalytic system would ensure a high catalytic activity and durability. Carbon blacks are widely used as supports for Pt particles in fuel cells because they offer a combination of good electrical conductivity, high specific surface area and low cost. However, graphitic carbon nanostructures such as nanotubes, nanofibers, nanocoils or nanocapsules have proved to be even more efficient as electrocatalyst supports [1-4]. This is because these nanostructures combine good electrical conductivity with an accessible surface area, as a result of which the three-phase boundary (catalyst-electrolyte-reactive) is maximized. In contrast, carbon blacks possess a high proportion of micropores (< 2 nm), which results in a low catalyst utilization as the mass transport is much slower in such micropores [5]. In addition, the smallest pores are not accessible to catalyst deposition, which may lead to particle agglomeration.

As already mentioned, it is important that the supports possess a high resistance to corrosion. Carbon oxidation is a significant drawback that diminishes electrocatalytic activity due to the rapid loss of active surface area [6] and changes to the pore morphology and pore surface characteristics [7]. One possible solution to this problem is to use graphitic carbon materials that exhibit greater resistance to oxidation than

carbon blacks [8-10]. There are many studies on the utilization of carbon nanotubes and other nanostructures (i. e. nanofibers) as supports for electrocatalysts. However, the synthesis methods employed to fabricate this materials are “complex”. Nowadays, there is a growing interest for “simple” synthetic strategies to obtain graphitic carbon nanostructures for use as electrocatalyst supports. In this sense, our group has undertaken a systematic investigation of different synthetic routes to produce, through catalytic graphitization, graphitic carbon nanostructures from a variety of precursors. We have prepared GCNs by using a cost-effective and widely available lignocellulosic material (sawdust) as precursor [11]. Likewise, we have analyzed the use of commercially available iron or cobalt organic salts (i. e. Fe (II) gluconate and Co (II) gluconate) as precursors [12]. A large number of research groups have demonstrated that the hydrothermal carbonization of saccharides constitutes a facile way to prepare carbonaceous microspheres with a high density of oxygen functional groups, which are useful in numerous applications and also as precursor for the synthesis of nanostructured inorganic materials [13, 14]. Bearing in mind the high density of oxygen functionalities we believe that these carbonaceous microspheres may constitute an excellent precursor for producing graphitic carbon nanostructures through the catalytic graphitization of metal impregnated samples. The results obtained so far have confirmed this hypothesis and have shown that graphitic nanostructures synthesised in this way have an exclusively nanocoil morphology [15]. This procedure constitutes a facile and novel synthetic route to produce graphitic carbon nanocoils, which could be produced on a large scale. Considering the structural properties of graphitic carbon nanocoils that are synthesized in this way (i. e. high graphitic order, absence of framework-confined pores and high external surface area), it is clear that that this material could be an excellent electrocatalyst support. Accordingly, in the present work, we investigate the

electrocatalytic performance of Pt nanoparticles supported on these graphitic carbon nanocoils (GCNC).

2. Experimental

2.1. Materials

The materials used were: hexachloroplatinic acid ($H_2PtCl_6 \cdot H_2O$, ca. 40% Pt, Aldrich), sulfuric acid 96% (Suprapur, Merck), methanol 99.8% (for chromatography, Merck), ethylenglycol (99.5%, Fluka), polivinylpirrolidone (PVP, Aldrich) AW 40,000, Nafion solution (5% w/w, Aldrich), carbon black (Vulcan XC-72R, BET area = 270 $m^2 \cdot g^{-1}$) supplied by Cabot Corporation and glassy carbon (0.3 cm diameter rod) from Carbone Lorraine. The water used in this work was obtained from an Elga Labwater Purelab Ultra system. The preparation of the GCNC consists of the following steps [15]: a) impregnation of the carbon microspheres with nickel nitrate (2 mmol $Ni \cdot g^{-1}$ C), b) heat treatment under N_2 at 900ºC and c) purification of the GCNC by liquid-phase oxidation. The GCNC samples obtained from glucose, sucrose and starch are denoted as NCG, NCS and NCA respectively.

2.2. Preparation of Pt/GCNC electrocatalysts and electrochemical measurements

Platinum catalysts were synthesized using the polymer-mediated polyol method [16]. Ethylene glycol was used as both the reducing agent and the solvent, and poly(vinylpyrrolidone), PVP, was used as polymer to prevent particle agglomeration. Briefly, the carbon support was dispersed in ethylene glycol and mixed with PVP dispersed in water (ethylene glycol/water solution: 3/1 (v/v); PVP:Pt = 0.15 (w/w)). Then, a predetermined amount of the Pt precursor $H_2PtCl_6.6H_2O$ was mixed with the dispersion and ultrasonicated for 10 min. The amount of Pt precursor was adjusted to ensure the desired Pt mass in the catalyst (v.g. 20 wt %). The Pt precursor concentration was kept constant at 0.002 M. The platinum ions were reduced by refluxing the polyol

solution (at ~140ºC) for 1 h under continuous magnetic stirring. The prepared catalysts were washed with acetone and ultra pure water in order to remove the PVP. Elimination of this compound was confirmed by XPS analysis. Finally they were dried at 40ºC in a vacuum oven overnight. The prepared catalyst was labeled by adding Pt/ to the nomenclature of the carbon samples. For purposes of comparison, platinum was also deposited on carbon black powder (Vulcan XC-72R, Cabot International) with a BET surface area of 270 $m^2 \cdot g^{-1}$, in the same conditions as for the GCNC.

The electroactive Pt surface area (ESA), was measured by cyclic voltammetry (CV) using an EG&G Mod. 175 Universal Programmer and a Potentiostat Mod. 101 HQ Instruments. A common three-electrode electrochemical cell was employed in these experiments while a 0.5 M H_2SO_4 solution was used as the electrolyte. An 0.3 cm diameter glassy carbon stick served as the working electrode (GC) and a platinum wire was used as the counter electrode. All the potentials were quoted against the reversible hydrogen electrode (RHE) immersed in the same solution as that used as the electrolyte. The GC was polished and washed ultrasonically with ultrapure water. The catalyst ink, consisting of the catalyst and a Nafion solution in acetone (10 mg catalyst/L and 33% Nafion), was dropped onto the GC and left to dry. Nitrogen was bubbled through the solution for the purpose of deaeration for 20 minutes prior to measurements being taken and this atmosphere was maintained throughout the experiments. The CVs were recorded at a scan rate of 50 $mV \cdot s^{-1}$ at room temperature. Prior to this, scans at 200 $mV \cdot s^{-1}$ up to 1.2V were performed in order to clean the Pt in the catalyst layer.

The electrocatalytic activity of the supported catalysts was tested by measuring the oxidation of methanol in 0.1 M CH_3OH (99.8%, Merck) in 0.5 M H_2SO_4 at 50 $mV \cdot s^{-1}$. The CV experiments were performed on a EG&G Potentiostat Galvanostat Mod. 263A.

2.3. Characterization

X-ray diffraction (XRD) patterns of the Pt catalysts were obtained on a Seifert JSO-DEBYEFLEX 2002 instrument, using CuKα radiation. The dispersion and size of the Pt particles were evaluated by means of the TEM images (with a JEOL (JEM-2010) microscope operating at 200 kV). Two to four hundred particles were measured for each sample in order to obtain statistically significant results. The loadings of Pt into the catalysts were determined by thermogravimetric analysis (TGA), which was performed in a Setaram 92-16.18 apparatus under air (Heating rate: 10 ºC/min). X-ray photoelectron spectroscopy (XPS) of the catalysts was carried out by means of a VG-Microtech Multilab spectrometer, using Mg Kα (1253.6 eV) radiation from a double anode with an energy flow of 50 eV.

3. Results and discussion

3.1. Physicochemical properties of Pt nanoparticles supported on the GCNs

Figure 1a shows a typical TEM image of a graphitic carbon nanocoil obtained from glucose. The particle which has a spiral shape (diameter ~ 100 nm) consists of a carbon ribbon with a width of approx. 10-20 nm. This material exhibits a high degree of crystallinity, as evidenced by the very well-defined (002) lattice fringes in the HRTEM image (Figure 1a, inset). This is confirmed by the XRD diffraction pattern, which contains intense peaks corresponding to the (002), (10), (004) and (110) diffraction characteristics of the graphitic framework (Figure 1b).

The TEM images obtained for the Pt nanoparticles supported on the GCNC clearly show that the nanosized catalyst is highly dispersed over the carbon support. This is exemplified by the TEM image in Figure 2a for the Pt/NCS catalytic system. A high dispersion of quasi-spherical Pt nanoparticles has been achieved in all the cases, confirming that PVP prevents the particles from agglomerating. As previously mentioned, this high dispersion is also due to the structure of the support. Surprisingly,

although these supports possess a surface area of 114-134 $m^2 \cdot g^{-1}$, which is half the Vulcan surface area (270 $m^2 \cdot g^{-1}$), a good dispersion has been achieved without the need for a functionalization step. This indicates that the GCNC contain abundant anchor sites for securing the Pt nanoparticles (π-sites and defects). This catalyst deposition method also allows a relatively narrow particle size distribution, as evidenced by the size histogram represented in Figure 2b. The mean Pt nanoparticle size is 3.0, 3.2 and 3.3 nm for NCG, NCA and NCS respectively, the standard deviation being 0.5 nm for NCG and 0.7 nm for NCA y NCS (see Table 1).

A typical Pt/GCNC XRD pattern is shown in Figure 2c. The diffraction peaks observed at 2θ~39.8, 46.3, 67.3 and 81.2º are characteristic of the face-centered cubic structure of Pt, while the peak that appears at 2θ~26º corresponds to the (002) reflection of the graphitic framework of GCNC. The average crystallite size (L) for the platinum nanoparticles was estimated by applying Scherrer's equation to the (111) diffraction peak:

$$L = \frac{0.9 \cdot \lambda}{\beta \cdot \cos\theta} \qquad (1)$$

where λ = 0.15406 nm and β is the full width at half maximum (FWHM) of the diffraction peak in radians. These values indicate that the Pt nanoparticles possess an average crystallite size in the 2.8-3.2 nm range, while for Pt supported on Vulcan the average crystallite size is slightly smaller (2.2 nm). These values agree well with those obtained by TEM inspection (see Figure 2b and Table 1).

The oxidation state of the deposited Pt nanoparticles was investigated by means of XPS spectroscopy. A representative Pt 4f core level spectrum for the Pt/NCG sample is shown in Figure 2d. The Pt 4f region exhibits a doublet from the spin-orbit splitting of the $4f_{7/2}$ (71.2 eV) and $4f_{5/2}$ (74.4 eV) states of metallic Pt(0). No peaks corresponding to Pt (II) or Pt (IV) were identified in the Pt/NCG catalyst. For the other catalytic

systems (v.g. Pt/NCA and Pt/NCS) similar results were obtained. This proves that the Pt ions are completely reduced when refluxed with ethylene glycol and that Pt(0) is the only active species in these catalytic systems.

The Pt loading of the Pt/GCNC catalysts was determined by thermogravimetric analysis. With this aim, the catalysts were heat-treated to 1000ºC under air. At this temperature, Pt is present in the form of PtO. The Pt loadings thus determined are in the 20.2-20.9 range (see Table 1). In Figure 3 the weight loss curves obtained for Pt/NCG and Pt/Vulcan during heating under air were compared. The weight loss profiles for Pt/NCS and Pt/NCA are similar to the one in Pt/NCG. It can also be seen that the oxidation of the carbon present in the Pt/NCG sample takes place at a temperature substantially higher (~100ºC) than that of Pt/Vulcan. This is of some importance because it indicates that the electrocatalysts based on GCNC have a greater stability against oxidation than the traditional electrocatalysts based on carbon blacks. What is more, this finding suggests that these electrocatalytic systems will have, under an oxidative environment (typical of fuel cells electrodes), a longer durability compared to Pt/Vulcan samples [17]. The superior resistance against corrosion observed for the GCNC is a consequence of their high crystallinity.

3.2. Electrochemical characterization of Pt nanoparticles supported on the GCNs

The electroactive Pt surface area (ESA) was measured by cyclic voltammetry (CV) in a solution of 0.5 M H_2SO_4 (scan rate: 50 $mV \cdot s^{-1}$, potential range: 0.06-1.2V). The steady-state voltammograms of the Pt/NCG and Pt/NCS catalysts are shown in Figure 4a. Well-defined hydrogen and anion adsorption-desorption peaks on the different faces of the Pt nanoparticles are observed in the potential range of 0.06-0.4V vs. RHE. These voltammetric profiles are consistent with those of a polycrystalline Pt. The cyclic voltammogram of Pt/NCA is similar to that of Pt/NCS and Pt/Vulcan. However, the

profile of these three catalysts differs from that of Pt/NCG, indicating that the platinum nanoparticles in Pt/NCG have a different surface structure. The electroactive Pt surface area was estimated from the CV curves using the following equation:

$$\text{ESA } [\text{cm}^2 \cdot \text{g}^{-1} \text{ Pt}] = \frac{Q}{m_{Pt} \cdot q_H^0} \quad (2)$$

where Q is the electrical charge (mC) obtained by integration of the voltammetric curve between 0.05V and 0.45V after the correction of the double layer charge, m_{Pt} [g Pt] is the actual loading of Pt into the catalyst, and q_H^0 is the charge for a monolayer of one electron adsorption-desorption process on Pt equal to 0.210 $mC \cdot cm^{-2}$ [16, 18].

The Pt/GCNC catalysts possess an ESA value in the 67.2-85.0 $m^2 \cdot g^{-1}$ Pt range (see Table 1). Only Pt/NCS has an ESA lower than Pt/Vulcan (73.6 $m^2 \cdot g^{-1}$ Pt). However, the utilization of Pt (assuming that the Pt particles are spherical and applying the diameter estimated by TEM) is higher in all the Pt/GCNC (79-94%) than in Pt/Vulcan (68%). This indicates that the Pt particles are more accessible in the case of Pt/GCNC. This is due to the fact that the GCNC do not possess any framework-confined porosity [15], so their entire surface area is external and therefore of easy access. We recently obtained similar results for catalysts made up of Pt nanoparticles deposited on carbon nanostructures obtained from pine sawdust [11] and Fe (II) and Co (II) gluconates [12].

The efficiency of the supported Pt catalysts as anodic materials in DMFC was examined by means of cyclic voltammetry experiments. Figure 3b shows the cyclic voltammograms during the 14th cycle of room-temperature methanol oxidation on the Pt/NCG and Pt/NCS electrocatalysts in a 0.1 M CH_3OH + 0.5 M H_2SO_4 solution at the rate of 50 $mV \cdot s^{-1}$. The shape of the CV curves is typical of methanol electrooxidation over platinum nanoparticles. The onset potential of methanol electrooxidation on Pt/GCN catalysts occurred at around 0.40 V, which shows a slightly positive shift with

respect to that of Pt/Vulcan (0.39 V). Similarly, the maximum peak current in the anodic sweep was achieved at 0.79-84 V for Pt/GCNs and 0.77 V for Pt/Vulcan. Therefore, the overpotential for methanol oxidation is slightly higher in the case of Pt/GCNC than for Pt/Vulcan. However, the potential of methanol oxidation for Pt/GCNs are lower than that of other catalysts supported over carbon materials [19-21]. In the cathodic sweep, another oxidation peak due to methanol re-oxidation was observed at 0.68-0.69 V for Pt/GCNs and 0.68 V for Pt/Vulcan. The potential range between 0.06 and 0.30 V shows that adsorption processes are inhibited on the platinum surface. However, for both electrocatalysts this blockage is very similar. The electrocatalytic activity was evaluated as the current per gram of platinum at the maximum of the anodic peak in the forward scan, after subtracting the double layer contribution, $\mathbf{I_f}$, and the values are indicated in Table 1. Although the Pt/GCNC possess a higher catalytic activity than that reported in the literature for electrocatalysts made up of Pt supported on other forms of graphitic carbon (e.g. multiwalled carbon nanotubes [25-27]), only the catalytic activity of Pt/NCG is higher than that of Pt/Vulcan. This may be a consequence of the different surface structure of the Pt particles deposited on NCG compared to those deposited on NCA and NCS (see inset of Figure 4a) and those deposited on Vulcan (the corresponding voltammogram in a 0.5 M H_2SO_4 solution can be seen in reference [11]). It is well documented that electrocatalytic activity, as well as the poisoning of the Pt surface, will depend on the crystallographic structure of the Pt microcrystallites deposited on the supports [25-28].

4. Conclusions

Pt nanoparticles in the 3-3.3 nm range were highly dispersed over graphitic carbon nanocoils synthesized by catalytic graphitization of carbon spherules obtained from the hydrothermal carbonization of sucrose, glucose and starch. The dispersion was achieved

without the need for a functionalization step for the GNCC, since these supports contain abundant anchor sites for the catalyst particles. A polymer mediated-polyol method was used to deposit the Pt nanoparticles. Compared to the Pt/Vulcan catalyst which was prepared in the same way, the Pt/GCNC catalysts exhibited a higher utilization of Pt, with electroactive surface areas in the 67-85 $m^2 \cdot g^{-1}$ Pt range. Moreover, these Pt/GCNC show a high catalytic activity towards methanol electrooxidation, with values reaching 201 $A \cdot g^{-1}$ Pt. It should also be noted that the Pt/GCNC electrocatalysts show a superior resistance against oxidation compared to the Pt/Vulcan sample. Thus, this catalytic system should be more durable.

Acknowledgments. The financial support for this research work provided by the Spanish MCyT (MAT2008-00407, MAT2007-60621 and FEDER) is gratefully acknowledged. M.S. and C.S. acknowledge the assistance of the Spanish MCyT for the award of a FPU.

5. References

[1] E.S. Steigerwalt, G.A. Deluga, D.E. Cliffel, C.M. Lukehart, J. Phys. Chem. B. 105 (2001) 8097.

[2] W. Li, C. Liang, W. Zhou, J. Qiu, Z. Zhou, G. Sun, Q. Xin, J. Phys. Chem. B. 107 (2003) 6292.

[3] S. Han, Y. Yun, K. Park, Y. Sung, T. Hyeon, Adv. Mater. 15 (2003) 1922.

[4] T. Hyeon, S. Han, Y. Sung, K. Park, Y. Kim, Chem. Int. Ed. 42 (2003) 4352.

[5] H. Liu, C. Song, L. Zhang, J. Zhang, H. Wang, D.P. J. Wilkinson, Power Sources 155 (2006) 95.

[6] E. J. Antolini, Mater. Sci. 38 (2003) 2995.

[7] K.H. Kangasniemi, D.A. Condit, T.D. J. Jarvi, Electrochem. Soc. 151 (2004) E125.

[8] L.M. Manocha, A. Warrier, S. Manocha, D.D. Edie, A.A. Ogale, Mater. Sci. Eng. B 132 (2006) 121.

[9] F. Su, J. Zeng, X. Bao, Y. Yu, J.Y. Lee, X.S. Zhao, Chem. Mater. 17 (2005) 3960.

[10] L.A. Montoro, J.M. Rosolen, Carbon 44 (2006) 3293.

[11] M. Sevilla, C. Sanchís, T. Valdés-Solís, E. Morallón, A.B. Fuertes, J. Phys. Chem. C 111 (2007) 9749.

[12] M. Sevilla, C. Salinas-Martínez de Lecea, T. Valdés-Solís, E. Morallón, A.B. Fuertes, Phys. Chem. Chem. Phys. 10 (2008) 1433.

[13] X. Sun, Y. Li, Langmuir 21 (2005) 6019.

[14] W. Wang, S. Xiong, L. Chen, B. Xi, H. Zhou, Z. Zhang, Crystal Growth & Design 6 (2006) 2422.

[15] M. Sevilla, A.B. Fuertes, Mater. Chem. Phys., 2008, doi:10.1016/j.matchemphys.2008.07.046.

[16] M. Chen, Y. Xing, Langmuir 21 (2005) 9334.

[17] D.A. Stevens, J.R. Dahn, Carbon 43 (2005) 179.

[18] R. Woods, Electroanal. Chem. Interf. Electrochem. 49 (1974) 217.

[19] D-J. Guo, H-L. Li, J. Power Sources 160 (2006) 44.

[20] H. Tang, J. Chen, L. Nie, D. Liu, W. Deng, Y. Kuang, S. Yao, J. Colloid. Interf. Sci. 269 (2004) 26.

[21] J.J. Niu, J.N. Wang, Electrochim. Acta 53 (2008) 8058.

[22] Y. Mu, H. Liang, J. Hu, L. Jiang, L. J. Wan, Phys. Chem. B. 109 (2005) 22212.

[23] Y-T. Kim, T. J. Mitani, Catal. 238 (2006) 394.

[24] S-F. Zheng, J-S. Hu, L-S. Zhong, L-J. Wan, W-G. Song, J. Phys. Chem. C 111 (2007) 11174.

[25] C. Lamy, J.M. Leger, J. Clavilier, R. Parsons, J Electroanal. Chem. 150 (1983) 71.

[26] X.H. Xia, T. Iwasita, F. Ge, W. Vielstich, Electrochim. Acta 41 (1996) 711.

[27] A. Tripković, S.L.J. Gojković, K.D.J. Popović, J.D. Lović, J. Serb. Chem. Soc. 71 (2006) 1333.

[28] T.H.M. Housmans, A.H. Wonders, M.T.M. Koper, J. Phys. Chem. B 110 (2006) 10021.

Legends

Figure 1. (a) TEM image of a carbon nanocoil obtained from glucose (Inset, HRTEM image showing the lattice fringes typical of graphitic materials); (b) XRD pattern for a glucose-based GCNC sample.

Figure 2. (a) TEM image of the Pt/NCS catalyst; (b) size histogram of Pt nanoparticles deposited on NCS; (c) XRD pattern of the Pt/NCS sample and (d) Pt 4f photoelectron spectrum of Pt/NCG.

Figure 3. TGA curves of the Pt/carbon catalysts (Heating rate: 10 ºC·min^{-1}, air atmosphere).

Figure 4. (a) Cyclic voltammograms of the Pt/NCG and Pt/NCS catalysts in a 0.5 M H_2SO_4 solution at 50 mV·s^{-1}. Inset: zoomed view of the hydrogen adsorption potential. (b) Cyclic voltammograms during the 14th cycle of room-temperature methanol oxidation on the Pt/NCG and Pt/NCS catalysts in 0.1 M CH_3OH in 0.5 M H_2SO_4 at 50 mV·s^{-1}.

Table 1. Physical properties and catalytic activities towards the methanol oxidation of Pt/GCNC electroctalysts

Sample	Pt (wt %)	Pt particle size (nm)		ESA ($m^2 \cdot g^{-1}$ Pt)	I_f ($A \cdot g^{-1}$ Pt)
		XRD	TEM *		
Pt/NCG	20.2	2.8	3.0 (±0.5)	85.0	201
Pt/NCA	20.6	3.0	3.2 (±0.7)	82.6	178
Pt/NCS	20.8	3.2	3.3 (±0.7)	67.2	168
Pt/Vulcan	20.9	2.2	2.6 (±0.5)	73.6	192

* The values for the standard deviations are given in parentheses

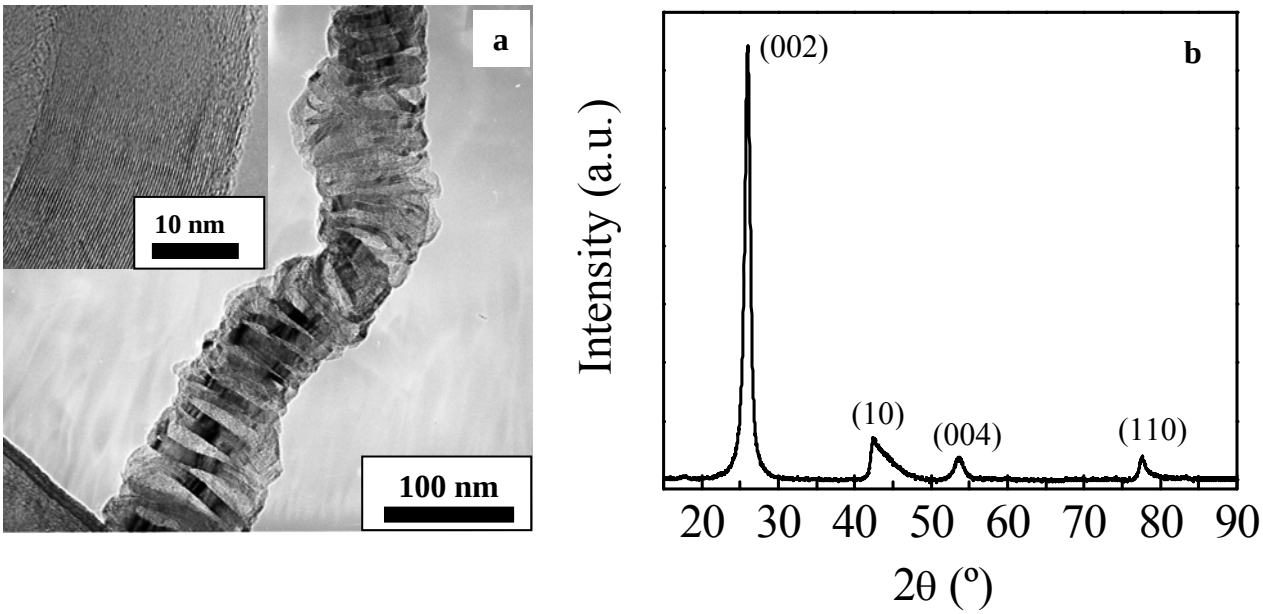

Figure 1. (a) TEM image of a carbon nanocoil obtained from glucose (Inset, HRTEM image showing the lattice fringes typical of graphitic materials); (b) XRD pattern for a glucose-based GCNC sample.

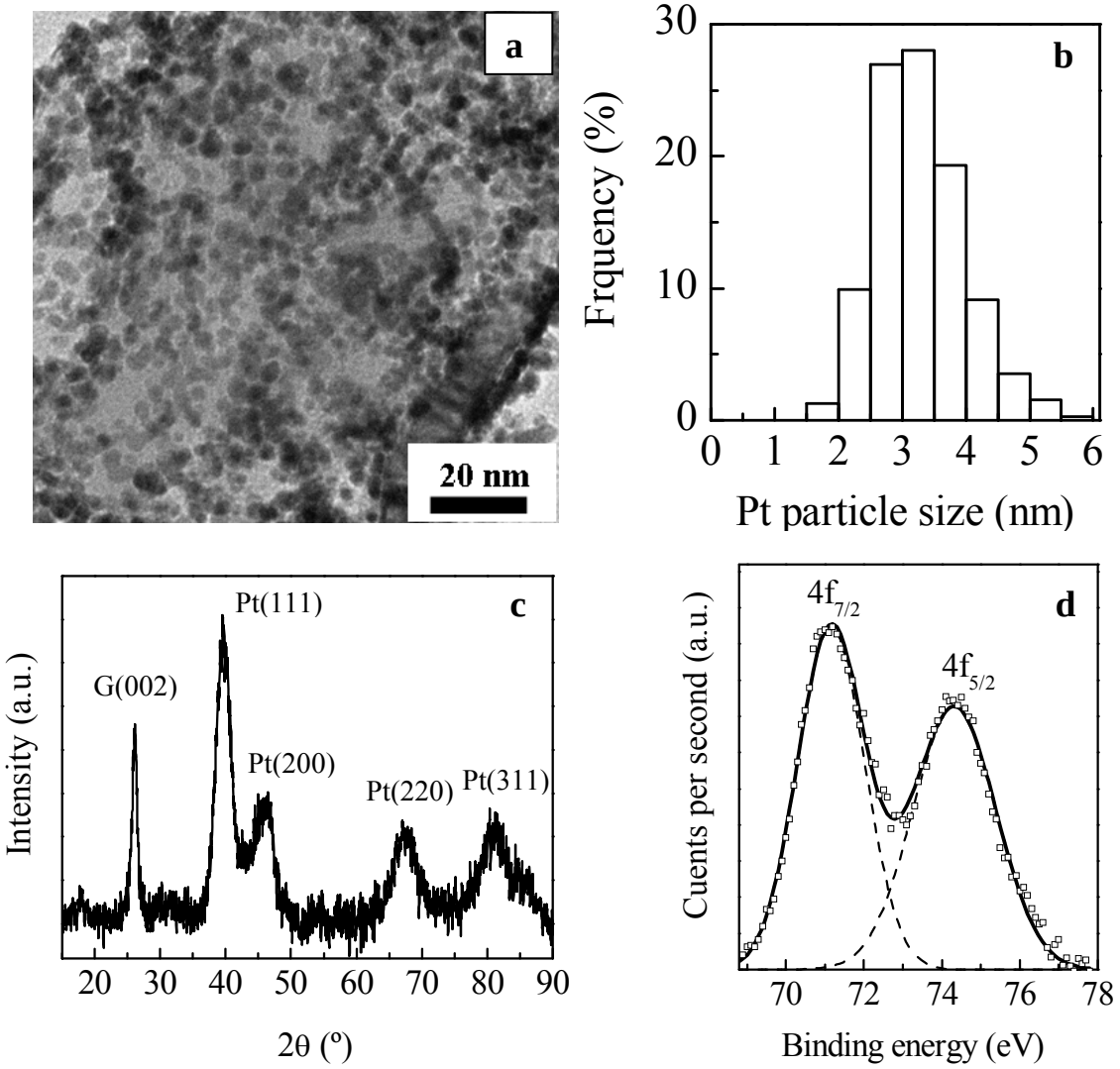

Figure 2. (a) TEM image of the Pt/NCS catalyst; (b) size histogram of Pt nanoparticles deposited on NCS; (c) XRD pattern of the Pt/NCS sample and (d) Pt 4f photoelectron spectrum of Pt/NCG.

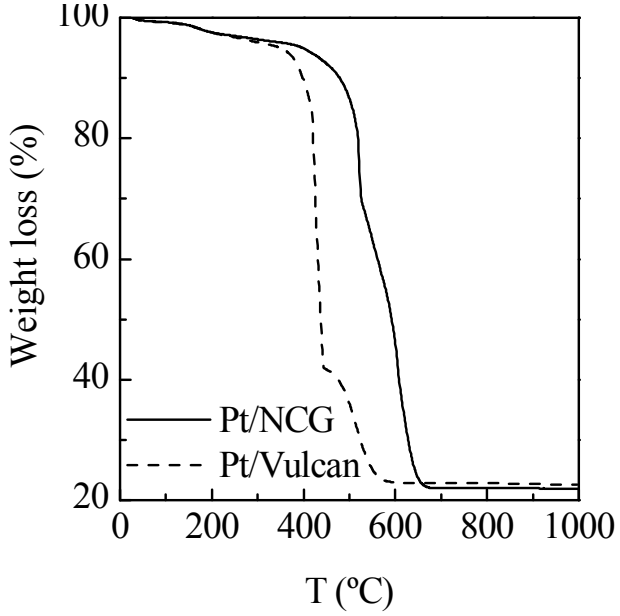

Figure 3. TGA curves of the Pt/carbon catalysts (Heating rate: 10 ºC·min^{-1}, air atmosphere).

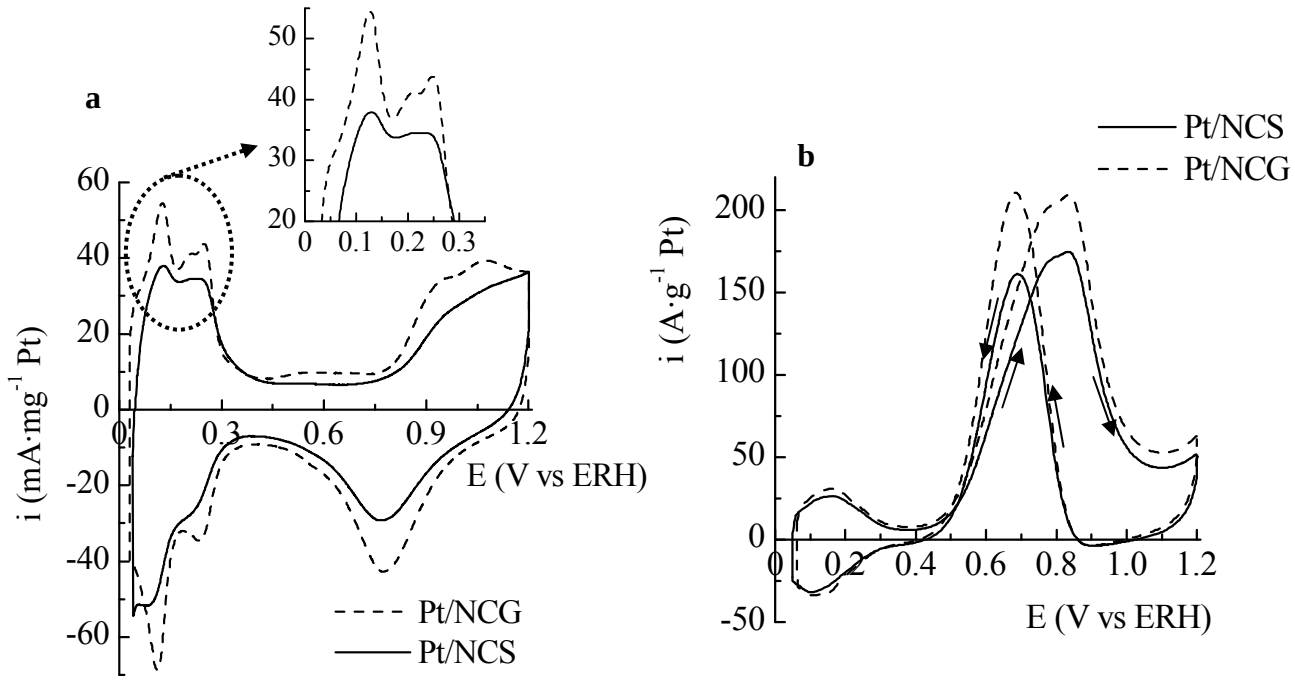

Figure 4. (a) Cyclic voltammograms of the Pt/NCG and Pt/NCS catalysts in a 0.5 M H_2SO_4 solution at 50 $mV \cdot s^{-1}$. Inset: zoomed view of the hydrogen adsorption potential. (b) Cyclic voltammograms during the 14th cycle of room-temperature methanol oxidation on the Pt/NCG and Pt/NCS catalysts in 0.1 M CH_3OH in 0.5 M H_2SO_4 at 50 $mV \cdot s^{-1}$.